Mott and Efros-Shklovskii Variable Range Hopping in CdSe Quantum Dots Films

Heng Liu, Alexandre Pourret,[†] and Philippe Guyot-Sionnest*

James Franck Institute, The University of Chicago, 929 E. 57th Street Chicago, Illinois 60637. [†]Current address: Laboratoire Photons Et Matiére (UPMC-CNRS) ESPCI, 75005 Paris, France.

ARTICLE

ABSTRACT The model of variable range hopping conductivity predicts a crossover between Mott and Efros-Shklovskii as a function of temperature and density of states. This is observed using monodispersed CdSe colloidal quantum dot 3D solids where the density of states at the Fermi level is varied by electrochemistry. At low density of states, both below the lowest state ($<0.4e^-$/dot) and in the conductivity gap between the first and second state ($2e^-$/dot), the temperature dependence of the conductivity shows the 1/4 exponent of Mott hopping. At other fillings up to $6e^-$/dot, the conductivity shows the 1/2 exponent of Efros-Shklovskii hopping. The non-Ohmic conductivity is also found to be explained quantitatively by the variable range hopping model.

KEYWORDS: CdSe quantum dots film · ES-Mott variable range hopping crossover · low temperature · electrochemistry

Monodispersed colloidal quantum dots (QDs) are attractive building blocks to create novel solids.[1] By controlling the Fermi level and the nature of the interdot region, the solids can exhibit Ohmic conductivity.[2] The conductivity is so far thermally activated[3−10] and deviates from Arrhenius behavior, ln $G \sim T^{-1}$, at low temperatures. For monodispersed CdSe and PbSe quantum dot films, Efros-Shklovskii (ES) variable range hopping (VRH)[11] accounts well for a $T^{-1/2}$ temperature dependence. Alternative pictures have been proposed. A "cotunneling"[6] model has been proposed for weakly coupled Au nanoparticle films to explain an identical 1/2 exponent, and a novel exponent of 2/3 was proposed to account for the temperature-dependent conductivity for ZnO nanocrystal films. Developing the appropriate model of conductivity is of practical relevance as conductive quantum dot solids are increasingly being investigated for thin film solar cells,[12] transistors,[9] or photodetectors.[13] VRH has long been studied in the context of disordered semiconductors,[11,14] and it makes several specific predictions about the nonlinear bias dependence[4] and the magnetoresistance that have been qualitatively confirmed for nanocrystal solids.[15] A further prediction of VRH is a crossover between two different temperature-activated behaviors. For a given density of state, VRH should evolve from the Mott regime, $T^{-1/4}$, at higher temperature to the ES, $T^{-1/2}$, regime, when the temperature is lower than the width of the Coulomb gap.[16] This crossover has been observed with doped bulk semiconductors, at fixed doping levels by decreasing the temperature, by changing the doping level using impurities[17,18] or using optical excitation.[19] Here, monodispersed CdSe QDs charged by electrochemistry and monitored spectroscopically allow one to vary quantitatively the density of states (DOS) over an order of magnitude without changing the system's disorder and composition.[16] This allows observation of the crossover between the two regimes as a function of DOS and temperature. ES-VRH also accounts quantitatively for the non-Ohmic regime at high bias.

VRH was originally developed for lightly doped semiconductors where the conductance is proportional to the probability of tunneling between sites separated by a distance r:

$$G \propto P \propto \exp(-2r/\xi - \Delta E/k_B T) \qquad (1)$$

ξ is the localization length, which characterizes the tunneling probability between nearest sites; r is the hopping distance; ΔE is the energy difference between the initial and final sites.

Mott[14] pointed out that the energy difference ΔE is related to r as $\Delta E \sim 1/g_0 r^D$ if there is a constant DOS g_0 near the Fermi surface, where D (1, 2, or 3) is the dimension

*Address correspondence to pgs@uchicago.edu.

Received for review June 18, 2010 and accepted August 12, 2010.

Published online August 18, 2010.
10.1021/nn101376u

© 2010 American Chemical Society

of the materials. Maximizing the probability leads to Mott's Law:

$$G \propto \exp(-(T_M/T)^{1/(D+1)}) \quad (2)$$

In 3D, ln G is linearly proportional to $T^{-1/4}$ and[12]

$$T_M = \frac{21.2}{k_B g_0 \xi^3} \quad (3)$$

This $T^{-1/4}$ Mott's Law has been observed in various classes of lightly doped semiconductors. Nevertheless, a large body of literature reported $T^{-1/2}$ instead of Mott's Law regardless of the dimension of the materials. Efros and Shklovskii[11] argued that the Coulomb interaction would open a soft gap in the DOS g_0 which leads to

$$G \propto \exp(-\sqrt{T_{ES}/T}) \quad (4)$$

In 1, 2, or 3 dimensions, T_{ES} is given by[11]

$$T_{ES} = \frac{\beta e^2}{\kappa k_B \xi} \quad (5)$$

κ is a macroscopic dielectric constant and β is a numerical constant of the order of unity (for 3D, $\beta = 2.8$).

The width of a Coulomb gap is determined by the unperturbed DOS g_0, $\Delta = e^3\sqrt{g_0}/\kappa^{3/2}$. Therefore, if $k_BT \gg \Delta$, the Coulomb effect becomes negligible and the conductivity crosses over from ES to Mott. In 3D, the ES-Mott crossover temperature can be written as[18]

$$T_{cross} = 16T_{ES}^2/T_M = \frac{5.9e^4 g_0 \xi}{\kappa^2 k_B} \quad (6)$$

RESULTS AND DISCUSSION

For the sample for which data are shown here, the CdSe nanocrystals' (NCs) diameter is ~6.2 nm, with a narrow size distribution (~7%). The first and second electron shells are 1Se, which can be occupied by $2e^-$, and $1P_e$, which can be occupied by $6e^-$. The films are drop-cast from a hexane/octane solution on Pt interdigitated electrodes with 10 μm spacing (Abtech Scientific Inc.). The dried films are immersed 30 s in an ethanol solution of 1% 1,7-diaminoheptane to replace the ligands with shorter molecules and improve conductivity. The films are rinsed with ethanol and baked in the oven at 90 °C for 30 min. The films are approximately 30 layers thick, as determined by the optical density. Inside a glovebox, the sample is placed in an airtight electrochemical cell with an electrolyte (0.1 M tetrabutylammonium perchlorate in propylene carbonate) and sandwiched between sapphire windows. A silicon diode and a heater are embedded into the aluminum body of the cell. The cell is cooled in an optical He flow cryostat, and the film is charged electrochemically around 210 K, which is close to the freezing point of the electrolyte. The electrochemistry brings the positive counterions next to the dots to compensate for the dots' negative charge. Once the electrolyte is frozen, the ions remain in place, enforcing the local charge of the dots to remain, as well. Also, around 210 K, charge decay, with disconnected electrodes, is much slower than the time required to establish a charging level. This leads to a homogeneous Fermi level as evidenced by the observation of a clean drop in conductivity when the $1S_e$ state is fully occupied.

The filling number n (the average number of electrons per dot) is determined by the optical bleach spectrum and its integration following the procedure described in ref 20. Some charge may be lost during the cooling, and the spectroscopy is noisy when the electrolyte is frozen due to scattering. This prevents a very accurate determination of charges in the frozen state, and we estimate the accuracy on the values of n given in the text at ~10%.

When a charging level is set and measured at 210 K, the cell is disconnected from the potentiostat and cooled below 160 K to keep the charges inside the film. Conductance measurements at any charging level are done only below 110 K. Conductance *versus* voltage curves are taken from 4.2 to 10 K at high biases to measure the nonlinear response. The Ohmic conductance G is measured with a fixed low voltage bias (<200 mV) as the cell is warmed from 10 to 110 K at a rate around 0.05 K/s. After warming the cell back up to 210 K, another charging level is selected and measured, and the procedure is repeated. Several charging and cooling cycles can be performed without measurable deterioration.

As compared to other methods, the electrochemical charge injection in the porous 3D quantum dot solids affords a reversible, uniform, and high level of charging per dot. Figure 1a shows a 3D plot of the conductance G against $T^{-1/2}$ and n. It demonstrates the shell filling previously seen only in cyclic voltammetry with the electrolyte in its liquid state.[2] The conductance increases as the $1S_e$ state starts to be occupied, decreases when the $1S_e$ shell has been filled (dark cyan line), and increases again as the $1P_e$ shell starts to be occupied. The conductivity gap at $1S_e$ filling becomes deeper at lower temperature. The gap is deep enough that the Ohmic response, easily measured at 15 K for $n \sim 1$, cannot be measured at that temperature for $n \sim 2$. An extrapolation of the data in Figure 1 leads to an estimated 1000-fold conductance drop from $n \sim 1$ to $n \sim 2$ at 15 K. The deep conductivity gap, or low dark current, between the $1S_e$ and $1P_e$ level opens up opportunities for mid-infrared photoconductivity based on the intraband transition and for future investigations. It is important to note that the lowest resistance of the sample (highest doping level at highest temperature) is ~0.2 MΩ, which is much larger than any expected contact resistance. Therefore, a two-point measurement is appropriate in the experiment.

Figure 1b−e shows the temperature-dependent conductance curves for selected charging levels. For some charging, log G is linear on the $T^{-1/2}$ graph; for others, it is linear on a $T^{-1/4}$ graph, and for some, log G follows neither exponents.

The exponent ν in the $\exp(-(T^*/T)^\nu)$ relation is objectively determined by the slopes of the logarithmic derivative $w = d(\log G)/d(\log T)$ plotted in Figure 2, against temperature on the double logarithmic scale[21] with corresponding error bars. The best fit of the slope directly gives the exponent ν. At most charging levels, the temperature-dependent conductance shows a single coefficient close to 1/2, but at low charging, the coefficient is close to 1/4. Figure 3 shows the characteristic temperatures T_{ES} and T_M data points in the respective ranges of applicability.

At $n = 0.4$, 2.3, and 2.5, the conductance shows an intermediate behavior, with a crossover from 1/4 to 1/2 exponent at ~ 80, 60, and 60 K, respectively. Besides predicting the crossover, VRH makes a quantitative prediction of the crossover temperature with eq 6. Using the values of $T_{ES}$and T_M in their respective range of applicability away from the crossover, eq 6 gives the crossover temperatures as 64, 54, and 53 K at $n = 0.4$, 2.3, and 2.5, respectively, in excellent agreement with the experiment.

According to eq 3, the Mott temperature is given by the DOS and localization length, such that knowing the DOS can be used to extract the localization length. The DOS in the quantum dot solids is determined by the distance between the dots, the energy separation between the levels of the dots, and the broadening arising from energy polydispersity. The DOS is then modeled with Gaussian distributions of standard deviations of 30, 60, and 80 meV for $1S_e$, $1P_e$, and $1D_e$, respectively. The width of $1S_e$ taken to be the room temperature luminescence width and the other widths are in proportion to the confinement energy, such that the ratio of width over confinement energy is constant for each state. From the optical spectra at 210 K, the energy separation between $1S_e$ and $1P_e$ is estimated to be ~230 ± 30 meV. A random close packing with 7 nm (the sum of diameter of NC, 6.2 nm, and the length of ligands, 0.8 nm) center to center separation is used. The resulting DOS is shown in the inset of Figure 3. At the conductivity gap between $1S_e$ and $1P_e$, the DOS is 1.0×10^{19} eV^{-1} cm^{-3}. Using eq 3 and the measured T_M of 4.3×10^7 K at that charging level, the localization length is $\xi = 0.8$ nm. Choosing $1S_e-1P_e$ energy separations of 200 or 260 meV changes the estimated DOS somewhat and leads to $\xi = 0.7$ or 1.1 nm, respectively. This localization length is significantly smaller than the dot separation d. The localization length defined in eq 1 characterizes the overlap of the wave functions between different sites, which does not need to be the same as the size of nanocrystals. Approximately, the overlap between nearest neighbor dot states is given by

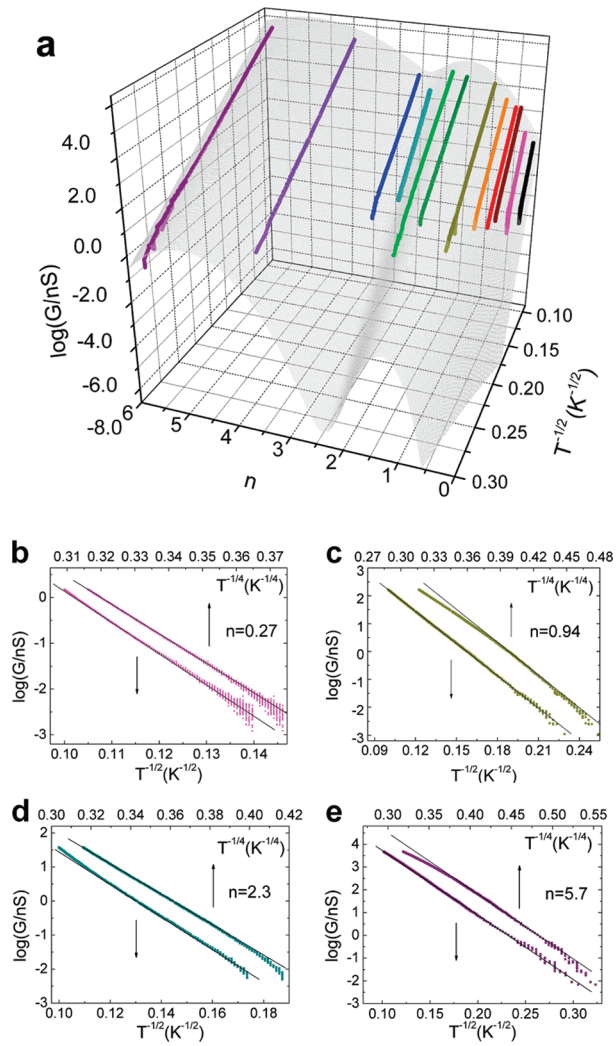

Figure 1. (a) Conductance G as a function of $T^{-1/2}$ and n. The lines are experimental data, and the background surface is a guide for the eye. There is a deep conductance gap between $1S_e$ and $1P_e$ at $n \sim 2$. (b−e) Same data set plotted *versus* $T^{-1/2}$ and $T^{-1/4}$ for different n indicated on each figure.

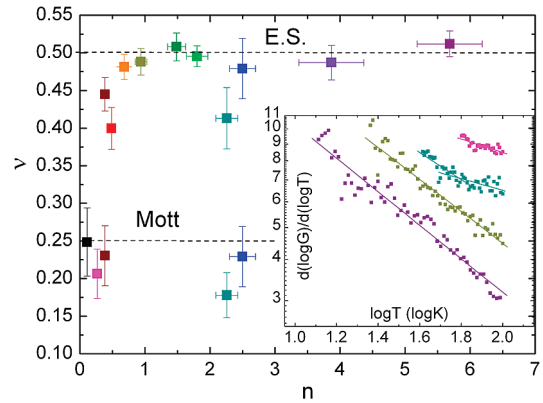

Figure 2. Exponent ν *versus* n. For $n = 0.4$, 2.3, and 2.5, two exponents are seen for different temperature ranges. The color scheme is the same as Figure 1. Inset: temperature dependence of the logarithmic derivative $d(\log G)/d(\log T)$ plotted on the double logarithmic scale for the data shown in Figure 1b−e.

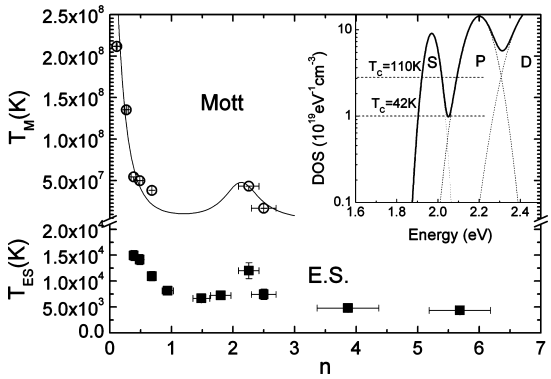

Figure 3. Effective temperature T_{ES} (solid squares) model and T_M (open circles) *versus n*. The line is the guide for the eye. The inset is the simulation of DOS in the system.

$\exp(-2d/\xi) \sim 10^{-6}$. Therefore, the system is in the weak coupling limit. An estimated maximum value of the mobility at high temperature is $\mu \sim (ed^2/h) \times \exp(-2d/\xi) \sim 10^{-4}$ cm^2/V/s (see Supporting Information). The overlap is small but nevertheless consistent with mobilities reported previously for this sample preparation.[2]

Figure 3 shows that the ranges where Mott applies are quite narrow. This is also consistent with the value of the localization length. With $\xi = 0.8$ nm, eq 6 indeed predicts that ES behavior applies across the full temperature range (10−110 K) as long as the DOS is larger than 2.6×10^{19} eV^{-1} cm^{-3}. As the system enters the ES regime, consistency requires further that an identical localization length should be obtained from the data. The localization length in the ES regime can be obtained from eq 5 and the measured T_{ES} using an estimated dielectric constant κ. However, it can also be obtained independently of an estimated dielectric constant using the non-Ohmic conductance at high bias. In this regime, the electron transport becomes field-driven and weakly temperature-dependent with a conductance tending asymptotically to $\exp(E^*/E)^{-1/2}$, where E is the electric field. $E^*$and T_{ES} are proportional as[4]

$$E^* = \frac{k_B}{2e\xi} T_{ES} \tag{7}$$

Figure 4 shows that the measured E^* and T_{ES} for several chargings follow a linear relationship. With eq 7, this suggests that the localization length is not very sensitive to the levels being charged. This is consistent with the high tunneling barrier due to the alkane ligands between dots. The slope is 4×10^4V m^{-1} K^{-1}, giving a localization length $\xi = 1.1$ nm, which is in very good agreement with the length in the Mott regime. In a previous study,[4] a discrepancy of 4 was reported between the measured and calculated E^*, and this was because the localization length was arbitrarily chosen as the radius of the QD. We can now correct this discrepancy and report that the VRH model quantitatively applies to the non-Ohmic regime, as well.

Around half-filling of $1S_e$ states, given the $T_{ES} = 8 \times 10^3$ K, and using the localization length $\xi = 1.1$ nm, eq 5 implies that the dielectric constant κ is ∼6. This is only slightly larger than the optical dielectric constant of the film measured to be ∼3.5 and therefore quite reasonable. As shown in Figure 3, there is a ∼3-fold variation of T_{ES} observed across different charging levels. This observation of the variation of T_{ES} as a function of charging is robust, seen for all samples studied. A similar but smaller effect was previously reported[4] and tentatively attributed to a change in dielectric constant in eq 5. However a 3-fold increase in the dielectric constant is not easily justifiable. The electronic polarizability of the film must increase as oscillator strength is transferred from the visible interband transition to the infrared intraband transitions, but estimates suggest only a ∼10% increase.[22] Possibly the increased cationic local concentration at higher charging level may play a role, but it does not explain the upturn in T_{ES} near the conductivity gap. Alternatively, a simulation study[23] has shown that the Coulomb gap parabola narrows after introducing spin degeneracy. Further degeneracy of the $1P_e$ energy levels may narrow the gap even more. The variation of T_{ES} with charging level therefore remains to be explained.

Given the localization length (∼1 nm) and using eq 6, a phase diagram of the Mott and ES regimes as a function of DOS and temperature is shown in Figure 5. At higher temperature, one should see nearest neighbor hopping (NNH) with Arrhenius T^{-1}. NNH is expected when the optimized hopping distance r_{opt} is of the order of the nearest neighbor distance a: $a/\xi \sim \Delta E_{nearest}/k_BT$.[24] Given the DOS and localization length, estimations show that NNH should only happen above ∼100 K, and indeed, the experiment does not display NNH between 10 and 100 K. Previous work extended to higher

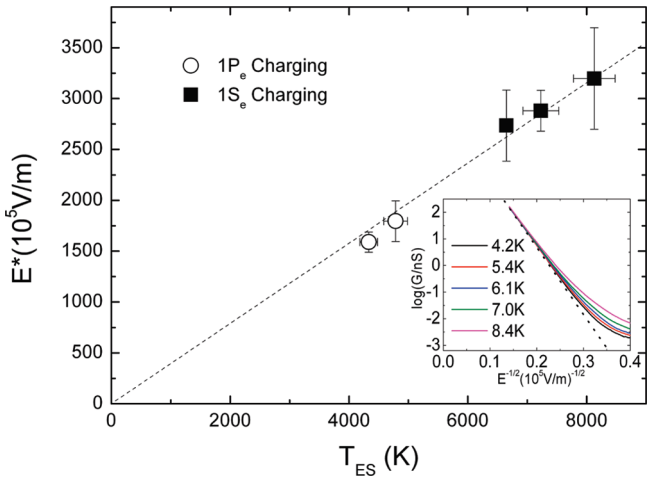

Figure 4. Effective electrical field E^* against effective temperature T_{ES} in the ES regime. The solid squares (open circles) are for the Fermi level in $1S_e$ ($1P_e$) states. The dashed line is the linear least-squares fit. Inset: one set of conductance data plotted *versus* $E^{-1/2}$ at different temperatures.

temperatures has already shown the onset of the Arrhenius behavior.[4]

In the context of NC films, the 1/2 exponent has been observed for other semiconductor systems[8] as well as for monodispersed metal[6] and magnetite nanocrystal arrays.[5,7] Although VRH could apply to all of these systems,[11] there are alternative models. There is a nearest neighbor hopping model with a specific distribution of barrier widths and Coulomb blockade energies such as developed for granular metals, but it leads to a different non-Ohmic prediction and cannot account for the 1/4 exponent.[25] There is a recent "cotunneling" model which will now need to be tested as thoroughly as VRH.[6] A novel exponent of 2/3, independent of charging density, has been recently reported for ZnO NCs film.[10] This exponent does not appear in the present study and prior studies on CdSe and PbSe QDs. The 2/3 exponent was explained by VRH but with a model for an activation based on energy fluctuations.[10] The ZnO NC films in ref 10 did not display state filling, reflecting greater polydispersity in size and coupling, as possibly evidenced by the large red shift (~0.2 eV) and broadening upon film formation, while mobilities remained low. One should carefully and broadly test the alternative model because artificial exponents, including 2/3, can arise from series resistances between inhomogeneous regions of different T_{ES}.

In summary, by electrochemically tuning the charging level of monodispersed CdSe QDs from 0.1 to 6e$^-$/dot, the Ohmic conductance of the CdSe QD films exhibits both Mott (low DOS) and ES (higher DOS) VRH in the 10−110 K range. The variable range hopping model quantitatively accounts for (i) the temperature range

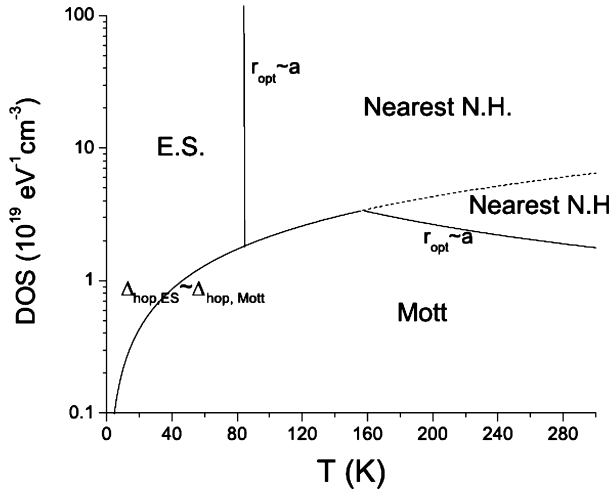

Figure 5. Phase diagram. The ES-Mott crossover temperature is determined by eq 6, and the nearest neighbor hopping (Nearest N. H.) takes place when the optimized hopping distance is of the order of nearest neighbor distance.

where the $T^{-1/4}$ and $T^{-1/2}$ regimes are observed within the range of charging levels studied, (ii) the similar value of localization lengths obtained in both regimes, and (iii) the nonlinear *I*/*V* curves. This ensemble of results provides a striking confirmation of the applicability of the VRH model to the NC systems. The variation of T_{ES} with different charging levels remains to be explained. With the diaminoheptane ligands used here, the localization length is ~1 nm, therefore much smaller than the dots. Different interdot material and spacing allow an increase in the localization length, and a promising avenue is to determine if the conduction regime changes as the localization length becomes of the order of the dot size.

METHODS

The CdSe nanocrytals (NCs) for which data are shown are prepared as follows: 27 mg of cadmium acetate (Aldrich) and 80 mg of myristic acid (Sigma) are dispersed in 3 mL of 1-octadecene (ODE) (Aldrich). After degassing at 100 °C, the temperature is raised to 250 °C under argon until all of the solids dissolved in the solution. Then 7 mg of selenium powder and 3 mL of ODE are added to the solution that is degassed at 120 °C. The solution is then heated rapidly to 220 °C under argon, when 1.5 mL of oleylamine is injected to provide ligands to CdSe NCs. The solution is kept at 230 °C for several minutes. Additional growth is done by adding 1 M TOP Se and 0.1 M cadmium 2,2-dimethyl butyrate in ODE into the solution dropwise.

The electrolyte is 0.1 M tetrabutylammonium perchlorate in propylene carbonate. The anhydrous propylene carbonate (Aldrich) is used as received. The tetrabutylammonium perchlorate (Aldrich) is dried under vacuum 100 mTorr overnight.

Acknowledgment. We are grateful to A. Pandey for many enlightening discussions and suggestions in NC synthesis. The research was supported by the DOE under Grant No. DE-FG02-06ER46326. The authors made use of shared facilities supported by the NSF MRSEC Program under DMR-0820054.

Supporting Information Available: More details on CdSe nanocrystals film preparation; SEM picture of the CdSe nanocrystals film, bleach spectra of CdSe film; similar crossover behavior on other CdSe and CdSe/CdS nanocrystal films; discussion on mobility and localization length. This material is available free of charge *via* the Internet at http://pubs.acs.org.

REFERENCES AND NOTES

1. Murray, C. B.; Kagan, C. R.; Bawendi, M. G. Synthesis and Characterization of Monodisperse Nanocrystals and Close-Packed Nanocrystal Assemblies. *Annu. Rev. Mater. Sci.* **2000**, *30*, 545–610.
2. Yu, D.; Wang, C.; Guyot-Sionnest, P. n-Type Conducting CdSe Nanocrystal Solids. *Science* **2003**, *300*, 1277–1280.
3. Zabet-Khosousi, A.; Dhirani, A.-A. Charge Transport in Nanoparticle Assemblies. *Chem. Rev.* **2008**, *108*, 4072–4124.
4. Yu, D.; Wang, C.; Wehrenberg, B. L.; Guyot-Sionnest, P. Variable Range Hopping Conduction in Semiconductor Nanocrystal Solids. *Phys. Rev. Lett.* **2004**, *92*, 216802.
5. Zeng, H.; Black, C. T.; Sandstrom, R. L.; Rice, P. M.; Murray, C. B.; Shouheng, S. Magnetotransport of Magnetite Nanoparticle Arrays. *Phys. Rev. B* **2006**, *73*, 020402.
6. Tran, T. B.; Beloborodov, I. S.; Hu, J.; Lin, X. M.; Rosenbaum, T. F.; Jaeger, H. M. Sequential Tunneling and Inelastic Cotunneling in Nanoparticle Arrays. *Phys. Rev. B* **2008**, *78*, 075437.
7. Xu, K.; Qin, L.; Heath, J. R. The Crossover from Two Dimensions to One Dimension in Granular Electronic Materials. *Nat. Nanotechnol.* **2009**, *4*, 368–372.

8. Wehrenberg, B. L.; Yu, D.; Ma, J.; Guyot-Sionnest, P. Conduction in Charged PbSe Nanocrystal Films. *J. Phys. Chem. B* **2005**, *109*, 20192–20199.
9. Talapin, D. V.; Murray, C. B. PbSe Nanocrystal Solids for n- and p-Channel Thin Film Field-Effect Transistors. *Science* **2005**, *310*, 86–89.
10. Houtepen, A. J.; Kockmann, D.; Vanmaekelbergh, D. Reappraisal of Variable-Range Hopping in Quantum-Dot Solids. *Nano Lett.* **2008**, *8*, 3516–3520.
11. Shklovskii, B. I. Efros, A. L. *Electronic Properties of Doped Semiconductors*; Springer-Verlag: Berlin, 1984; pp 202−251.
12. Hillhouse, H. W.; Beard, M. C. Solar Cells from Colloidal Nanocrystals: Fundamentals, Materials, Devices, and Economics. *Curr. Opin. Colloid Interface Sci.* **2009**, *14*, 245–259.
13. Edward, H. S. Solar Cells, Photodetectors, and Optical Sources from Infrared Colloidal Quantum Dots. *Adv. Mater.* **2008**, *20*, 3958–3964.
14. Mott, N. F. S. *Conduction in Non-Crystalline Materials*, 2nd ed.; Clarendon Press: Oxford, 1993; Vol. ix, p 150.
15. Yu, D.; Wehrenberg, B. L.; Yang, I.; Kang, W.; Guyot-Sionnest, P. Magnetoresistance of n-Type Quantum Dot Solids. *Appl. Phys. Lett.* **2006**, *88*, 072504.
16. Zhang, J.; Shklovskii, B. I. Density of States and Conductivity of a Granular Metal or an Array of Quantum Dots. *Phys. Rev. B* **2004**, *70*, 115317.
17. Zhang, Y.; Dai, O.; Levy, M.; Sarachik, M. P. Probing the Coulomb Gap in Insulating n-Type CdSe. *Phys. Rev. Lett.* **1990**, *64*, 2687.
18. Rosenbaum, R. Crossover from Mott to Efros-Shklovskii Variable-Range-Hopping Conductivity in In_xO_y Films. *Phys. Rev. B* **1991**, *44*, 3599.
19. Moreira, H. S.; Sampaio, J. F.; Alves, E. S.; de Oliveira, A. G. Electron Concentration Dependence of the Coulomb Gap in AlGaAs:Si. *Phys. Rev. Lett.* **1998**, *80*, 1706.
20. Jha, P. P.; Guyot-Sionnest, P. Photoluminescence Switching of Charged Quantum Dot Films. *J. Phys. Chem. C* **2007**, *111*, 15440–15445.
21. Zabrodskii, A. G. The Coulomb Gap: The View of an Experimenter. *Philos. Mag. B* **2001**, *81*, 1131–1151.
22. Delerue, C.; Allan, G.; Niquet, Y. M. Collective Excitations in Charged Nanocrystals and in Close-Packed Arrays of Charged Nanocrystals. *Phys. Rev. B* **2005**, *72*, 195316.
23. Davies, J. H. Coulomb Gaps and Hubbard Gaps. *J. Phys. C: Solid State Phys.* **1984**, *17*, 3031–3043.
24. Yildiz, A.; Serin, N.; Serin, T.; Kasap, M. Crossover from Nearest-Neighbor Hopping Conduction to Efros-Shklovskii Variable-Range Hopping Conduction in Hydrogenated Amorphous Silicon Films. *Jpn. J. Appl. Phys.* **2009**, *48*, 111203.
25. Sheng, P.; Abeles, B.; Arie, Y. Hopping Conductivity in Granular Metals. *Phys. Rev. Lett.* **1973**, *31*, 44.